Predicting the rotation profile in ITER

C Chrystal[1], B A Grierson[2], S R Haskey[2], A C Sontag[3], F M Poli[2], M W Shafer[3], J S deGrassie[1]

[1]General Atomics, P.O. Box 85608, San Diego, California 92186-5608, USA
[2]Princeton Plasma Physics Laboratory, Princeton, New Jersey 08543-0451, USA
[3]Oak Ridge National Laboratory
P.O. Box 2008, Oak Ridge, Tennessee 37831-6169, USA

E-mail: chrystal@fusion.gat.com

Abstract. Determining the toroidal rotation for future tokamaks like ITER is a challenging and important problem. By combining empirical scalings for the intrinsic rotation at the top of the pedestal with the expected neutral beam torque and modeling of momentum transport, the toroidal rotation profile for ITER is predicted with TGYRO using TGLF (SAT0 and SAT1). On axis rotation exceeds 20 krad/s and the $\mathbf{E} \times \mathbf{B}$ shear is significant enough to reduce turbulent transport and significantly increase confinement and fusion power when comparing to cases that ignore the effect of rotation. The prediction of the rotation at the top of the pedestal is made with increased confidence due to experiments and modeling in DIII-D that have determined the importance of fast-ion and neutral particle transport effects on intrinsic rotation at this location. In particular, the effect of neutral particles on momentum transport in the pedestal region is found to be insignificant.

Submitted to: *Nucl. Fusion*

1. Introduction

Rotation is a key parameter in tokamak plasmas because it helps improve MHD stability[1, 2, 3, 4, 5, 6, 7], turbulent transport (due to $\mathbf{E} \times \mathbf{B}$ shear suppression[8]), impurity transport [9, 10, 11], and access to H-mode scenarios that lack ELMs[12, 13]. Therefore, predicting the rotation for future tokamaks is an important task that is the subject of this work. Future large tokamaks such as ITER pose a particular problem for rotation predictions because their large moment of inertia and practical limits on available neutral beam torque create a situation where this torque is not the clear dominant source of rotation as in many current tokamak scenarios. This increases the need for accurate models for all other non-neutral beam sources of angular momentum, but, currently, these sources are less understood.

Angular momentum can be driven inside the last closed flux surface (LCFS) without neutral beams due to some combination of: turbulence driven residual stress, Maxwell stress from MHD or other 3D fields, and neoclassical toroidal viscosity (NTV). All of these effects are the subject of current research. One of the robust features of intrinsic rotation profiles is the strong co-current rotation seen in the large majority of cases at or just inside the LCFS[14, 15, 16, 17, 18]. This feature is significant because it serves as the boundary condition for the rest of the rotation profile. Possible physical explanations for this feature include orbit loss, asymmetric transport of ions with co- and counter-current velocity, and residual stress. These complex effects have been covered in multiple reviews[19, 20, 21, 22]. Though these effects are considered good candidates for the main drivers of this rotation feature, this region of the plasma is one that may in principle be affected by the dynamics of fast-ion loss and the influence of neutral particles on momentum transport. The potential influence of these two effects must be understood because they will be reduced in ITER when compared to many current experiments due to the lower fast-ion content and decreased neutral penetration. Results from two experiments at DIII-D investigated these effects will be presented in this paper.

While the effects from self-generated and applied 3D fields are likely to be important for ITER, they can be highly nonlinear (e.g. mode locking). Accordingly, this work will ignore these effects to provide an initial rotation value that can serve as the basis for future work that investigates 3D field effects. Any experimental results in this work are carefully selected so that any 3D field effects are insignificant.

The rotation predictions of this work are made with a combination of models for the co-current intrinsic rotation feature at the top of the pedestal and modeling of the neutral beam torque and momentum flux. The pedestal top intrinsic rotation can be predicted from a database of measurements in multiple tokamaks that can be described by a small number of parameters[14, 23]. It is also possible to form reduced physics models that can predict the rotation and then test the results against a reasonably varied data set[24, 25, 26]. Lastly, a prediction can be made with dimensionless parameter scalings formed from dedicated dimensionless parameter scan experiments[27, 28]. Predictions from all three of these methods are taken into account to create a conservative boundary condition for the modeling of core rotation. The boundary conditions predicted by these different methods are similar from the perspective of modeling the core even though there are differences in the results underlying the predictions. The two DIII-D experiments that investigated the effect of fast-ions and neutral particles are also useful for gaining understanding of these differences.

Most previous predictions of the whole rotation profile for ITER have not included intrinsic rotation or a co-current rotation boundary condition[29, 30, 31]. Reference [32] is an exception that calculates an intrinsic rotation by using a relation between the heat flux and the residual stress. In that work, the boundary rotation is set to 0 and the turbulent momentum transport analysis is limited to taking the Prandtl number to be uniformly 1. In this work, as in [28], gyro-fluid modeling will be used to determine core transport of energy, particles, and, momentum such that the predicted fluxes match those of a transport simulation of an ITER baseline scenario. This modeling uses the full neutral beam torque of 35 $\mathrm{N} \cdot \mathrm{m}$ while the modeling of [28] only used 20 $\mathrm{N} \cdot \mathrm{m}$.

In this work, section 2 describes DIII-D results on the effect of fast-ions on the determination of the ρ_* scaling of intrinsic rotation, and section 3 describes DIII-D results on the effect of neutral particles in the edge on intrinsic rotation. Section 4 presents predictions of the ITER rotation profile and the effects of that rotation on ITER's performance. Section 5 discusses the viability of RMP ELM suppression in ITER given the rotation predicted at the top of the pedestal. Conclusions are presented in section 6.

2. ρ_* Scaling of Intrinsic Rotation

To make predictions for ITER, the underlying dependencies of the co-current intrinsic rotation feature at the top of

the pedestal need to be determined. A previous study in DIII-D that was executed within the dimensionless parameter scan formalism[33, 34] showed that the total intrinsic torque inside the pedestal ($\rho < 0.9$, with ρ being the normalized square root of toroidal flux within a flux surface), normalized by ion temperature, scaled as $\rho_*^{-1.6}$ ($\rho_* \equiv \sqrt{2mT}/ZeBa$) and the momentum confinement time, normalized by the Bohm time, at the top of the pedestal ($\rho = 0.9$) scaled as $\rho_*^{-0.4}$[28]. As explained in that work, these results were unexpected based on concepts of residual stress driven intrinsic rotation and results from database studies of intrinsic rotation, which found the intrinsic rotation at the top of the pedestal to scale as ρ_*^0[14] or ρ_*^1[23, 24]. The results of [25, 26] also show a scaling of ρ_*^1 if $L_\phi \sim a$, where L_ϕ is the radial scale length of electrostatic fluctuation intensity.

To investigate this discrepancy, an experiment directly measuring the intrinsic rotation of H-mode plasmas in a ρ_* scan was executed. Auxiliary power input came only from electron cyclotron heating (ECH), and short duration ($\approx$ 10 ms) neutral beam injections with nearly balanced torque were used to measure ion properties with charge exchange recombination spectroscopy (CER). The beam injections had nearly balanced torque, but measurements of rotation took into account indications of small prompt torque effects [35]. Past database results can be compared to the measurements of intrinsic Mach number in this experiment. In addition, dimensionless parameter scan results for the intrinsic torque and momentum confinement time can be compared to the measurements of core angular momentum in this experiment. The dimensionless parameter scan prediction from [28] is that $(\tau_{\rm int}/T)(t_\varphi T/B) \sim L_{\rm int}/B \sim \rho_*^{-1.9\pm0.9}$, with $\tau_{\rm int}$ being the intrinsic torque, t_φ being the momentum confinement time, and $L_{\rm int}$ being the intrinsic angular momentum. The results of these comparisons will help determine how the conflicting past results should be used to make a prediction for ITER.

For this experiment, toroidal field was varied from 1.3 T to 2.1 T with other parameters changed according to the procedure described in [33, 34]. The associated reduction in ρ_* is $\approx$ 27%. A comparison of several of the dimensionless parameters for the discharges that will be used for analysis is shown in figure 1 (q_{95} for all the discharges is 6.1). Aside from the change in $Z_{\rm eff}$, these results show that a reasonably good ρ_* scan was completed across the core of the plasma, where intrinsic angular momentum will be analyzed. Though ν_* and β are not exactly matched in any pair of low and high ρ_* discharges, the average difference between ν_* and β across multiple discharges is small.

The scaling of the normalized core angular momentum ($0.3 < \rho < 0.8$), and pedestal top ($\rho = 0.8$) Mach number (rotation speed normalized to sound speed) are shown in figure 2. The calculated scalings are derived from only the impurity rotation measurements, and their

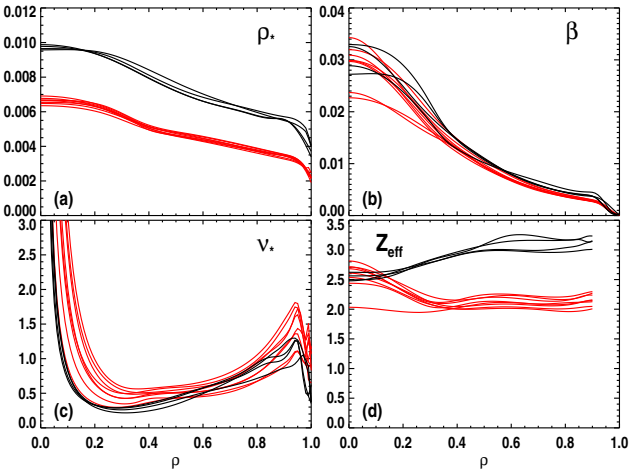

Figure 1. Key dimensionless parameters for several discharges used to study the dependence of intrinsic rotation in a ρ_* dimensionless parameter scan. As seen in (a), discharges with low (high) ρ_* are red (black). (b) β and (c) ν_* are held relatively constant. (d) $Z_{\rm eff}$ notably differed. Data shown comes from shots 168872, 168875, 168876, 168878, and 169015

relation to the main-ion (deuterium in this paper) rotation points are discussed in the last paragraph of this section. The $\rho_*^{-0.90\pm0.07}$ scaling of the core angular momentum has a smaller magnitude than the expectation ($\rho_*^{-1.9\pm0.9}$). This could be an indication that fast-ions present in the earlier study of intrinsic torque affected the measured ρ_* scaling (in that study, the core fast-ion fraction decreased with lower ρ_*[27]). To be consistent with the newly measured scaling, an increase in fast-ion content would need to decrease the measured intrinsic torque at higher ρ_*. This could be possible if there is significant counter-current torque created by fast-ion loss that is not properly accounted for in the transport modeling (an area of current fast-ion research). Another, difficult to rule out possibility is that intrinsic rotation plasmas created on DIII-D fundamentally differ from neutral beam heated plasmas (e.g. in transport regime and momentum confinement time) so that the underlying ρ_* dependence of intrinsic angular momentum is actually different.

Although the indications of this experiment are that the fast-ions may have contributed to the discrepancy between the dimensionless parameter scan and database results, a direct comparison between the ρ_* scaling of intrinsic Mach number at the top of the pedestal and database studies shows some discrepancy still remains. While [23, 24] found the Alfvén Mach number to scale as ρ_*^1, the present results shows a scaling of ρ_*^0, which agrees with the older result of [14]. Note that in a dimensionless parameter scan, Mach number and Alfvén Mach number have the same scaling to the extent β has been held constant.

The discrepancy between these scaling results is smaller than the discrepancy between the previous intrinsic torque results and the database studies. Any final resolution between these different results will likely require further

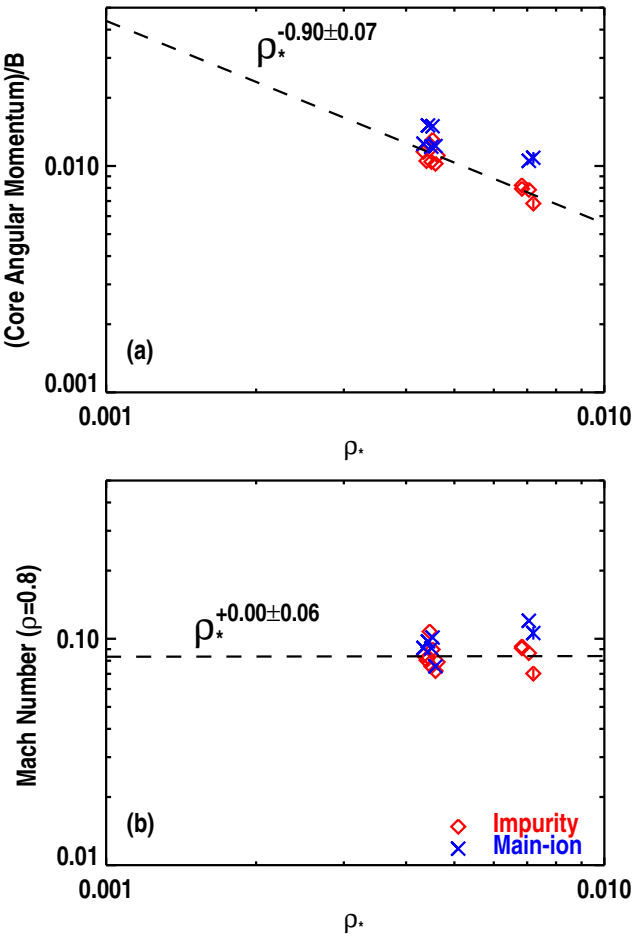

Figure 2. (a) The scaling of the integrated intrinsic angular momentum ($0.3 < \rho < 0.8$) normalized by the magnetic field, and (b) the Mach number at the pedestal top ($\rho = 0.8$) with ρ_*. Error bars shown only on points with largest ρ_* are representative. The normalized intrinsic angular momentum scales less strongly than expected from previous experiments while the Mach number shows no significant scaling. Both scalings are derived from the impurity rotation. The smaller data-set of main-ion measurements are on average larger because of the larger main-ion rotation.

investigation. The biggest weakness in database results is that they may be measuring the effect of a controlling parameter aside from ρ_* that is then projected onto a ρ_* axis. The biggest weaknesses of the dimensionless parameter scans performed in DIII-D is the narrow range over which ρ_* can be scanned and the potential for there to be a deficiency in how well the scan was performed. For instance, if the change in $Z_{\rm eff}$ were affecting the intrinsic rotation, or if some other, potentially unmeasured, dimensionless parameter were changing significantly. Special consideration for this last possibility is required in the case of intrinsic rotation at the top of the pedestal because this feature is the result of co-current momentum flowing across the LCFS. There is therefore a possibility that conditions in or near the scrape off layer are what truly determine this intrinsic rotation. Features in this region can be difficult to measure and may have unexpected co-linearities with ρ_* when executing a standard ρ_* scan (this specific concern is partially addressed in section 3). Lastly, when comparing the dimensionless parameter results to database studies, it must be said that the significance of any discrepancies between different dimensionless parameters investigations should be evaluated relative to the inherent scatter in the underlying data that makes up database studies. These two inescapable uncertainties are similar. While a single factor or ρ_* when projecting from DIII-D to ITER amounts to a factor of $\approx 1/4$, measurements of Mach numbers that scalings derived from databases predict to be the same can in fact differ by a factor of ≈ 2[23, 24, 26].

In DIII-D, measurements of main-ion rotation are available across the plasma profile[36, 37], however, analysis was difficult in this case because of the high ELM frequency and infrequent potential measurement times in these discharges. The main-ion rotation measurements are available for only one of the high ρ_* discharges. Because of this and the fact that no single high and low ρ_* set of discharges have a good match of ν_* and β (as discussed above), the main-ion data-set is not suited for determining the ρ_* scaling on its own. Aside from this difficulty, the results calculated from just the impurity rotation are more suitable to compare to previous results that also came from impurity measurements. It is still important to use the main-ion measurements as much as possible to gain confidence in how representative the impurity measurements are of the bulk plasma. For this reason, figure 2 also shows the main-ion results so their approximate scalings can be compared to the scalings derived from the impurity measurements. The main-ion data points are on average larger than the impurity results because of the main-ion rotation is $\approx$ 20% higher (5−10 km/s). The existing points also suggest that measured scalings with ρ_* would be less than the reported values if the main-ion rotation were available for the whole data-set.

3. Neutral Particle Investigations

As discussed at the end of section 2, the persistent discrepancies between different determinations of the ρ_* scaling of intrinsic rotation prompts investigation into the dependence of intrinsic rotation on other parameters that are not tracked and may not be held constant during a standard ρ_* scan. This section investigates the hypothesis that the neutral particles in the edge of the plasma have a significant effect on intrinsic rotation. Since neutral density is rarely measured in this region, unintentional variations in this parameter could be spoiling comparisons between different tokamaks and even different experiments on the same tokamak. This is an especially relevant issue to investigate because neutral penetration will decrease significantly in ITER relative to current tokamaks. If neutral particles are important for intrinsic rotation, the change in their properties must be accounted for when projecting current

results to ITER.

The most simplistic view of neutral particles effects on momentum in the edge is that a cold neutral coming from the wall enters the plasma, charge exchanges or ionizes, and then decreases the average angular momentum due to a combination of its own low speed and the potential loss of angular momentum as the warm ion escapes the plasma after being neutralized. Another possibility is that charge exchange occurs much more quickly than other processes such that a neutral coming from the edge would be more aptly described as an electron transferring many times from one warm ion to another and thereby causing a diffusion of those ions down the neutral density gradient, i.e. into the plasma. Calculations taking this mechanism into account show that it may contribute significantly to the intrinsic rotation near the edge of tokamaks[38, 39]. Additional possible effects include the combination of ionization location and drifts and the viscosity between neutrals and ions[40, 41], with some experimental indications of the latter effect being seen on the TCABR tokamak[42].

In DIII-D, in the absence of neutral density measurements, divertor closure was varied and taken to be a proxy for changes in the neutral density. The concept of divertor closure concerns the physical geometry of the first wall near the strike points and how well this wall is able to keep neutrals confined to the immediate vicinity of the strike points[43]. A more closed divertor traps recycling neutrals in the divertor region, decreases their penetration into the plasma, and reduces fueling of the pedestal from the ionization of recycling neutrals[44, 45, 46]. In DIII-D, a lower single null shape that puts its low field side strike point on the "shelf" has a more open divertor, and when it is mirrored vertically the first wall of DIII-D creates a more closed divertor. By simultaneously changing the magnetic field direction ($\mathbf{B} \times \nabla \mathbf{B}$ direction constant relative to X-point) and the location of the gas valve used to fuel the plasma, symmetric open and closed geometries can be used to investigate the effect of closure on otherwise similar plasmas. The open and closed shapes used in this experiment are shown in figure 3(a).

In this experiment, intrinsic rotation discharges were created in more open and closed configurations with a range of densities. The only significant auxiliary heating was from a constant $\approx$ 3 MW of ECH. Short duration neutral beam blips were used to measure ion properties in the same manner as described in section 2. A comparison of open and closed discharges supports the conclusion that neutral particles have a small influence on momentum transport. This is seen in figure 3 where the increased pedestal fueling in the more open case is evidenced by the higher electron density at the LCFS and the larger minor radius at which the maximum pedestal density is achieved. This is consistent with the presence of more neutrals in the main chamber where flux compression makes it easier for neutrals to enter the plasma, and represents a significant change in a

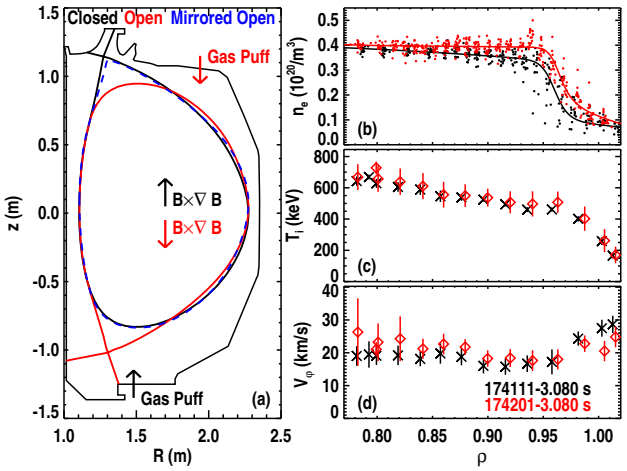

Figure 3. A comparison of two similar discharges with open (red) and closed (black) divertors, showing: (a) the shapes and gas puff locations (dashed blue is the open shape vertically mirrored), (b) the electron density profiles, (c) the deuterium temperature, and (d) the deuterium toroidal rotation. Though the change in neutral particle source has affected the electron density profile, no effect is seen in the ion temperature or rotation.

DIII-D pedestal for otherwise similar plasma parameters (both cases have very similar electron temperatures that reach $\approx$ 600 eV at the top of the pedestal). At the same time, the ion temperature and rotation (measured with main-ion CER[36, 37]) are essentially identical in this region. The unchanging ion temperature is important because intrinsic rotation in DIII-D is known to generally scale with ion temperature[47, 26]. The impurity temperature and rotation measurements (not shown) are also the same within error bars.

Additional evidence for a change in the neutral density in the two discharges compared in figure 3 is provided by modeling of these discharges with SOLPS[48, 49, 50]. The modeling results for the neutral deuterium density are shown in figure 4, and the results for the recycling particle source are shown in figure 5. Both results show that the neutral penetration and subsequent fueling are increased in the pedestal region for the more open configuration. This is consistent with the expectations and supports the conclusion that intrinsic rotation in DIII-D is not significantly affected by changes in the neutral density in the pedestal. Accordingly, there is experimental justification for ignoring this potential effect when projecting results to ITER.

This conclusion is further supported a coarse investigation of the discharges from this experiment. In the open and closed data sets, the correlation between intrinsic rotation and ion temperature at the top of the pedestal (for impurity measurements because main-ion measurements are not available for all these discharges) is very similar, as shown in figure 6. Also shown in this figure is the intensity of the D_α emission at the outboard midplane as measured by filterscopes. The increase in this signal for the more open di-

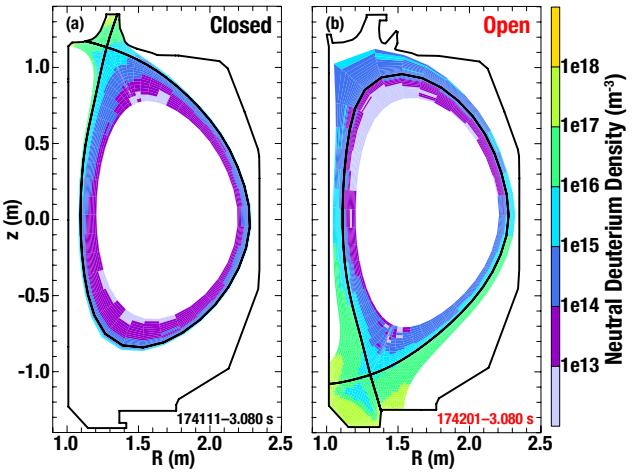

Figure 4. SOLPS modeling of neutral deuterium density for the (a) closed and (b) open configurations compared in figure 3. The more open configuration has increased neutral penetration and increased neutral density (by orders of magnitude) near the midplane of the plasma.

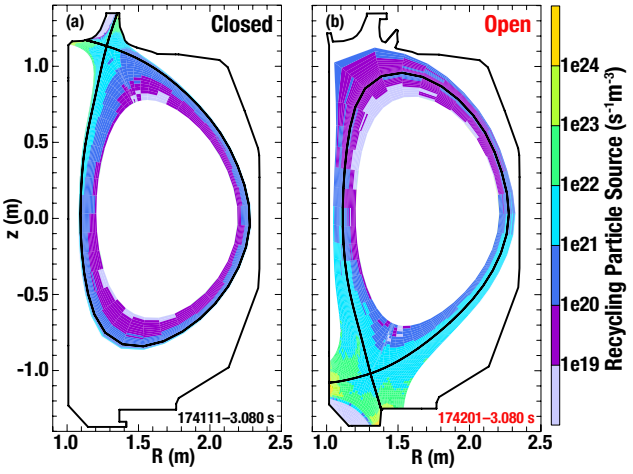

Figure 5. SOLPS modeling of recycling particle source for the (a) closed and (b) open configurations compared in figure 3. The more open configuration has an increased particle source from recycling in the pedestal that is consistent with the increased neutral density in that region.

vertor discharges is consistent with the increase in neutral density in this region due to the effects of divertor closure, though, D_α emissivity also depends on electron density and temperature.

A final piece of evidence consistent with this conclusion comes from the analysis of intrinsic rotation at the top of the pedestal as the divertor plasma detaches. This result is shown in figure 7. Here, it can be seen from the rollover in the ion saturation current measured by Langmuir probes near the strikepoint and the strong increase in the neutral pressure in the divertor region that the plasma begins to detach by 2.5 s[51]. Other results consistent with detachment include an increase of the electron density at the LCFS of 40% in the time range shown (measured by Thomson scattering) and a decrease of electron temperature

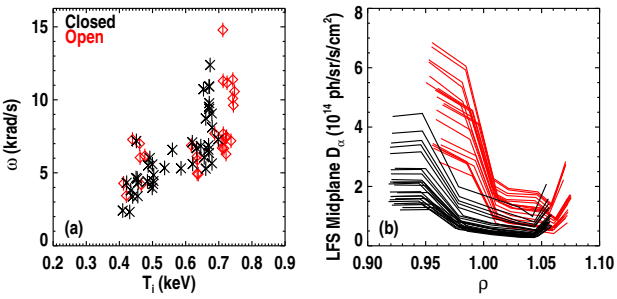

Figure 6. (a) Toroidal rotation frequency versus ion temperature at the top of the pedestal and (b) D_α emission on the outboard midplane of the plasma for several intrinsic rotation H-mode discharges with either open or closed divertor configurations. Discharges that used gas fueling to achieve detachment (and had uniformly higher D_α signals) are not included in (b).

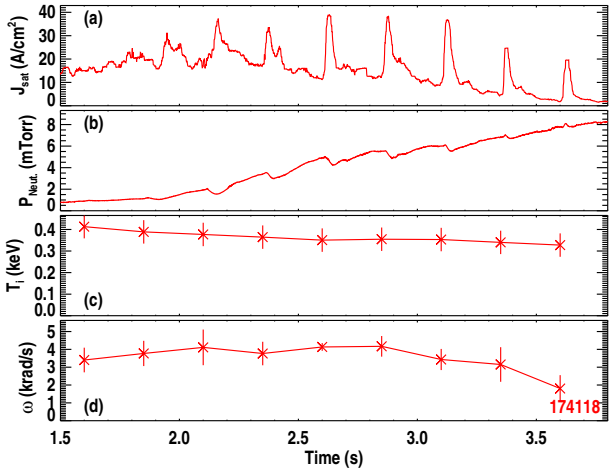

Figure 7. (a) Ion saturation current density at the strikepoint, (b) neutral pressure near the strikepoint, (c) pedestal top ion temperature, and (d) pedestal top toroidal rotation frequency for a discharge that enters a detached state. The J_{sat} increases transiently with each neutral beam blip, but the underlying trend shows rollover between 2 and 2.5 s, consistent with the beginning of detachment and the large increases in the nearby neutral pressure.

at the strikepoint to < 3 eV (measured by Langmuir probes). While the neutral pressure increases significantly in the divertor, the ion temperature and rotation at the top of the pedestal (measured again by impurity CER) remain almost constant. This is consistent with the conclusion that significant changes in neutral particle fueling in the pedestal do not significantly effect the intrinsic rotation.

4. ITER Modeling

The prediction of the rotation profile in ITER will be generated from self-consistent modeling of the energy, particle, and momentum transport with the boundary condition for the rotation informed by multiple past studies and the experimental results discussed in previous sections. The modeling begins with a predictive TRANSP[52] simulation of the ITER baseline scenario (15 MA, D-T, $Q \equiv$

P_{fus}/P_{aux} is nominally 10). In this simulation, EPED[53] is used to set the pedestal width and pressure. Electron density is set with a power law profile such that the profile is flat in the core while the ratios of core density to the pedestal and LCFS densities are 4/3 and 20/7, respectively. The whole profile is scaled so that the line averaged Greenwald density fraction is 0.85. Auxiliary power comes from 33 MW of neutral beam injection (NBI), 10 MW of ion cyclotron heating, and 6 MW of ECH (aimed to drive current at the $q = 3/2$ and $q = 2$ surfaces). The NBI provides 35 N · m of total torque. TRANSP determines the sources of energy, particle, and momentum, and GLF23[54] is then used to determine temperature and momentum profiles. These sources and profiles are used as the initial conditions in a TGYRO[55] simulation of temperature, density, and rotation profiles with transport being determined by TGLF[56] (for completeness, SAT0[57] and SAT1[58] will be used) and NEO[59]. In these simulations, TGYRO self-consistently computes the fusion energy and particle sources, but all other sources are fixed. This analysis was performed with the OMFIT integrated modeling framework [60]. The use of TGLF for ITER simulations for momentum transport is supported by studies of momentum transport in DIII-D[28] that found TGLF modeling (SAT0) to be relatively accurate for plasmas with lower q (the safety factor) and ν_*.

The TGYRO modeling is done at 7 radii equally spaced within $0.3 \leq \rho \leq 0.9$. The boundary conditions at $\rho = 0.9$ for temperatures and density come from the TRANSP simulation. The rotation boundary condition of 4 krad/s is formed from a set of recent predictions of the intrinsic rotation at the top of the pedestal in a ITER baseline H-mode. The chosen boundary condition is conservative in two ways: first it is a relatively small result among the set of all predictions, and second it does not include any effect from the neutral beam torque (however, note again that NTV torque is not included in this prediction). The predictions from [23], [26], [27], and [24] are 4, 4[61], 10, and 10 krad/s, respectively. If the results of section 2 are used to adjust the prediction from [27], the ≈ 10 krad/s becomes 3 krad/s. The results of section 3 provide justification for not adjusting any of these results based on the changing influence of neutral particles when going from present tokamaks to ITER.

The results of the TGYRO modeling are shown in figure 8. Results for both the SAT0 and SAT1 versions of TGLF are shown with and without the effect of rotation included. In the no rotation cases, the rotation profiles are set to be flat so that there is no $\mathbf{E}\times\mathbf{B}$ shear. The SAT1 model has incorporated information from a few computationally expensive multi-scale GYRO simulations and may yield more accurate results. However, the SAT0 model has been used for longer and subjected to more validation. For these reasons, the results of both are of interest. Using both models is also useful because common results can be identified as not something that is somehow peculiar to one particular model.

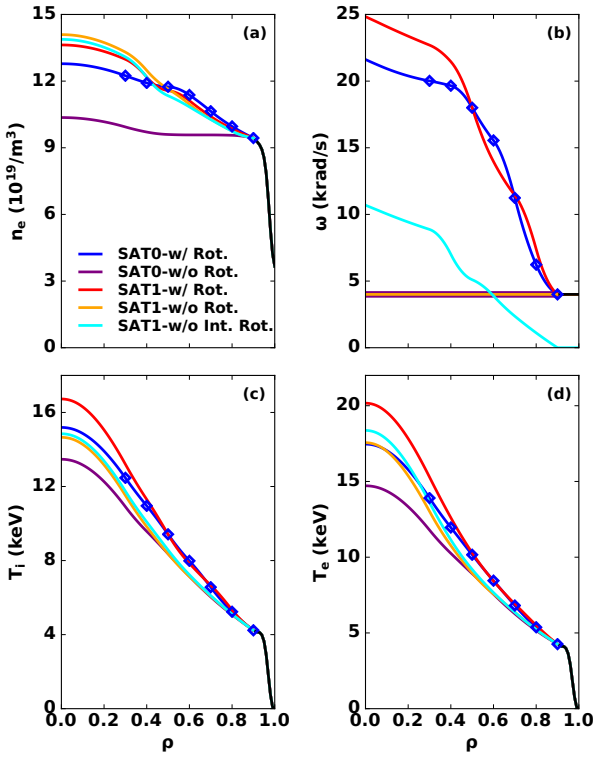

Figure 8. Predictions for profiles of (a) electron density, (b) toroidal rotation frequency, (c) ion temperature, and (d) electron temperature in a 15 MA ITER scenario. Predictions are made with both the SAT0 and SAT1 TGLF models with and without the effect of rotation being included. All the simulations are done at the same 7 radii that are shown in blue diamonds. The boundary condition for rotation is based on empirical intrinsic rotation predictions aside from the case with an assumed 0 krad/s boundary condition. The simulations that include intrinsic and neutral beam driven rotation have significantly increased performance due to the effect of $\mathbf{E}\times\mathbf{B}$ shear.

The SAT0 results are discussed first. Without rotation, a flat density profile and relatively low ion temperatures are predicted, and these result in a relatively low fusion power. Q is 4.6. However, the values of Q in this work should only be considered in a relative sense because these are not complete models of the ITER plasma. In particular, the D-T ratio is always taken to be perfect and radiated power is not being modeled self-consistently. When the rotation is allowed to increase due to the neutral beam torque, the $\mathbf{E}\times\mathbf{B}$ shear suppresses turbulent transport and increases the particle, energy, and momentum confinement times significantly. This yields a significant increase of fusion power, and Q rises to 9.5. The key factor in the increased confinement in this case is the influence of the $\mathbf{E}\times\mathbf{B}$ shear on the particle confinement. Figure 9 shows how the turbulent particle transport changes with $\mathbf{E}\times\mathbf{B}$ shear in the SAT0 simulation at a representative radii ($\rho = 0.6$). The $\mathbf{E}\times\mathbf{B}$ shear is scanned from 0 to

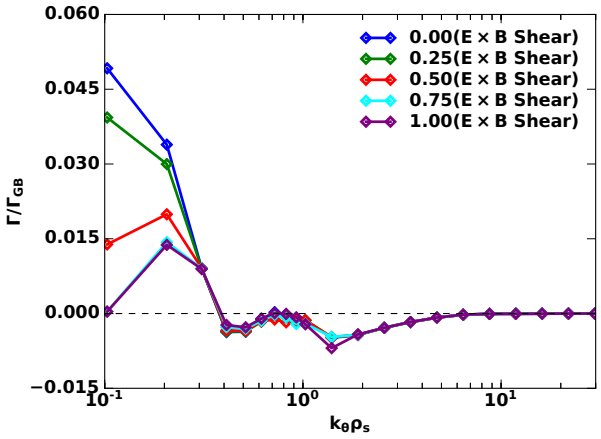

Figure 9. The gyro-Bohm normalized particle flux spectrum at $\rho = 0.6$ in the SAT0–with rotation ITER simulation from figure 8 with a scan of the $\mathbf{E} \times \mathbf{B}$ shear. As $\mathbf{E} \times \mathbf{B}$ shear increases, large outward flux from low-wavenumber modes is suppressed.

the value given by the rotation profile and the parallel flow shear is scaled self-consistently. The decrease in the outward particle flux from low wavenumber turbulence is clear. If there was no $\mathbf{E} \times \mathbf{B}$ shear, the outward particle flux from these wavenumbers would transport particles out of the core and force TGYRO to decrease the density peaking in order to match the target particle flux. The density peaking that is present also increases the core electron temperature which then increases the intermediate wavenumber turbulence which further increases the density peaking through increased inward particle flux. A similar phenomenology was observed in the modeling of a similar ITER scenario in in [62].

The SAT1 results show a final rotation profile that is similar to that of the SAT0 result. The on-axis rotation is only a few krad/s higher while the values in the mid-radius region are very similar. The main difference between the SAT1 and SAT0 results is tied to the fact that SAT1 predicts density peaking even without the effect of $\mathbf{E} \times \mathbf{B}$ shear. Due to this, the SAT1, no rotation case has a Q of 8.6 (compare to SAT0, no rotation Q of 4.6). The SAT1, with rotation simulation sees increased performance due to an increase in the energy confinement, with no appreciable change in the density profile. Q for this case is 11.1. The density peaking is actually slightly smaller in the SAT1 simulation with rotation because the increased energy confinement increases the outward particle transport. While the amount that the performance increases with rotation in the SAT0 and SAT1 cases differs, both increases are significant. The importance of rotation for ITER's performance is a robust component of both of these predictions.

Another SAT1 result is shown for a case without any intrinsic rotation (i.e., the boundary condition for rotation is set to be 0 krad/s). This case is useful for illustrating the importance of the intrinsic rotation through the inward transport of momentum with a pinch. While the core rotation still increases when compared to the initial condition due to the neutral beam torque, it can be seen that there is less rotation shear in the core than in the SAT1 case with intrinsic rotation. Q for this simulation is essentially unchanged from the SAT1, no rotation case (8.7 versus 8.6). Based on this result, it is expected that if the rotation boundary condition were increased by some amount above 4 krad/s, there would be an even larger increase in the rotation at the magnetic axis and an associated increase in the core rotation shear. At this point, it should be noted that the edge intrinsic rotation is not just important due to its interplay with any momentum pinch. Modeling effects of 3D magnetic fields requires knowing the radial electric field (and hence the rotation) near the edge.

All these simulations are done under the standard high-rotation ordering in TGYRO. That is, the radial electric field is taken to be solely a result of the toroidal rotation. For the simulations with rotation, the pressure gradient term presents a $< 10\%$ correction to the radial electric field determined by the rotation alone. This is true even in the cases with density peaking because the ion density peaking is not as extreme as the electron density peaking due to the influence of the fusion generated helium ions. In addition to the pressure gradient contribution to the radial electric field, poloidal rotation on the level of 1 km/s at mid radius represents an additional 10% effect.

A final important point to discuss for these simulations is the assumption inherent in setting a rotation boundary condition as has been done in the above simulations. When particle or momentum pinches transport momentum inward from the boundary, there is, by construction, no corresponding reduction in the total momentum at the boundary. Whether or not this represents the physical reality depends on the physical mechanism setting the co-current intrinsic rotation feature. If the intrinsic rotation mechanism works to hold rotation at a certain value, the boundary condition in this models is appropriate. However, if the intrinsic rotation is the result of a mechanism that generates a source of momentum that is independent of rotation, the boundary condition would need to be scaled down as momentum is transported into the core.

5. Implications for RMP ELM Suppression

Recent research efforts have focused on developing a RMP ELM suppression scenario at an ITER relevant level of rotation. These RMP ELM suppression investigations have led to the conclusion that the inward shift of the location where the radial electric field, E_r, crosses zero with lower rotation is the reason RMP ELM suppression cannot be achieved at very low levels of rotation[63] (though, a similar role for the zero crossing of the perpendicular electron flow has also been put forward[12]). In DIII-D, the lower limit appears to be $\approx$ 10 – 20 km/s ($\approx$ 5 –

9 krad/s) of co-current rotation at the top of the pedestal, as measured by impurity CER[63]. All else being equal, higher levels of rotation cause the radius where E_r crosses zero to shift outward, which is favorable for achieving RMP ELM suppression.

A simple estimate of the rotation required to achieve $E_r = 0$ can be made. Using the standard form for E_r and taking the general form of a divergence free velocity, $\mathbf{V} = \omega(\psi)R\hat{\varphi} + K(\psi)\mathbf{B}$, the condition for $E_r = 0$ is $\nabla P/nZe = \omega R B_\theta$. Note that the ω in this equation is not identical to the toroidal rotation frequency unless the poloidal rotation is zero. This relation can be used to find how the lower limit of rotation needed for RMP ELM suppression will scale. To that end, both sides of the equation are multiplied by $R\sqrt{T/m}/Ba$ to make it dimensionless. The result is:

$$-(\lambda_T^{-1} + \lambda_n^{-1})\rho_* q = M\epsilon, \quad (1)$$

where M is a Mach number ($R\omega/c_s$ with c_s being the sound speed), ϵ is the inverse aspect ratio (a/R), λ is the gradient scale length divided by the minor radius, and B was approximated as B_φ in the factor of q. If we assume the normalized gradient scale lengths are not changing and begin with the rotation of a DIII-D discharge with the ITER value of ϵ that achieved RMP ELM suppression, so long as the ITER rotation is lowered by at most a factor of $\rho_* q$, the toroidal rotation should be sufficient to create an acceptable location for $E_r = 0$. The factor of $\rho_* q$ is about 0.15 when comparing lower rotation RMP ELM suppression discharges in DIII-D and prospective ITER baseline discharges (with q_{95} only decreasing by 10% from DIII-D to ITER). Taking into account the Mach number normalization as well, the $5 - 9$ krad/s of pedestal top rotation required to maintain RMP ELM suppression on DIII-D scales to an ITER rotation frequency of $0.2 - 0.5$ krad/s. Physically, the lower required rotation for ELM suppression in ITER can be thought of as being a result of the larger gradient scale length and higher poloidal field (dimensionally) in ITER. Since the predictions for the pedestal top intrinsic rotation in this work are > 3 krad/s, the prospect for RMP ELM suppression in ITER appears to be good.

In DIII-D, the $5 - 9$ krad/s discharges were achieved with NBI torque that is typically deemed too large to be ITER relevant. However, total NBI torque comparisons are not relevant to discussions of the mechanism for ELM suppression that is dependent on the rotation in a small radial region. In fact, as discussed in [63], ELM suppression is lost when the NBI torque density in the edge is counter-current, even when the total torque is significantly co-current. This underlines the need to look at more than the total NBI torque when considering whether or not the toroidal rotation is relevant to ITER.

Though the calculation above looks favorable, further investigation of the effect of 3D fields on rotation is required. Even if it is assumed that error field correction can abrogate the effect of field ripple, as suggested by DIII-D experiments with the Test Blanket Module[64], the effect of the 3D fields applied for RMP ELM suppression still need to be taken into account. The rotation prediction of this work is necessary to form the initial condition upon which the NTV torque from the applied 3D field will act, and this investigation is left to future work.

6. Conclusions

The toroidal rotation profile for ITER has been predicted with a combination of empirical scalings of the co-current intrinsic rotation feature at the top of the pedestal and transport modeling of the core momentum flux due to the expected neutral beam torque in an ITER baseline scenario. The conservative estimate put forth for the intrinsic rotation at the top of the pedestal is 4 krad/s, and the modeled core rotation exceeds 20 krad/s when either the SAT0 or the SAT1 TGLF model is used. The increase in rotation across the core improves confinement there through $\mathbf{E} \times \mathbf{B}$ shear, increasing core energy confinement enough to have a significant effect on the fusion performance. This is especially true for the SAT0 results where the $\mathbf{E} \times \mathbf{B}$ shear is also key for increasing core density peaking. The addition of toroidal rotation increases fusion power with a constant auxiliary power by $\approx 30 - 100\%$ in these results.

These predictions of core rotation were also found to be dependent on the rotation boundary condition chosen due to the importance of the momentum pinch, and the 4 krad/s boundary condition was made with increased confidence due to recent experimental investigations on DIII-D that made use of main-ion CER measurements. One reason for this confidence was the result of the first experiment on DIII-D looking directly at the influence of edge neutrals on intrinsic rotation, which showed that the influence was negligible. This result is important because it is known that the neutral particles in ITER will not penetrate as far into the plasma as they do in current tokamaks. This increased confidence is also a result of the convergence of several predictions for the intrinsic rotation at the top of the pedestal in ITER, and the investigation of the effect of fast-ions on previous DIII-D measurements of intrinsic torque in a ρ_* dimensionless parameter scan. These results reduced the discrepancy between previous studies on the ρ_* scaling of intrinsic rotation. While some discrepancies in the results remain (and future work should still try to reconcile this issue), the biggest outstanding issue is the interplay between rotation and 3D fields.

The most likely scenario for ITER $Q = 10$ operation involves the use of 3D fields to suppress ELMs with RMP ELM suppression. While it was shown that even low rotation values at the top of the pedestal appear compatible with RMP ELM suppression, the achieved rotation may be below this low value due to effects on rotation from the resonant and non-resonant components of the applied 3D fields. These effects, including the nonlinear interplay

between the radial electric field and NTV torque, need to be studied more carefully due to their potential to affect the ability of ITER to meet its goals. In addition, as the ITER modeling in this work showed, low rotation at the top of the pedestal can significantly reduce the peak rotation achieved due to the effect of the pinch on the momentum confinement. This presents another reason to study the interplay between 3D fields and the rotation so that, hopefully, these harmful effects can be mitigated or avoided altogether.

Acknowledgments

The first author would like to acknowledge useful conversations with A W Leonard, A L Moser, H Q Wang, C. Paz-Soldan, and J. McClenaghan. This material is based on the work supported by the U.S. Department of Energy, Office of Science, Office of Fusion Energy Sciences, using the DIII-D National Fusion Facility, a DOE Office of Science user facility, under Award Nos. DE-FC02-04ER54698, DE-AC02-09CH11466, and DE-AC05-00OR22725. DIII-D data shown in this paper can be obtained in digital format by following the links at https://fusion.gat.com/global/D3D_DMP.

References

[1] Garofalo A, Bialek J, Navratil G, Sabbagh S, Turnbull A, Chu M, Groebner R, L a Haye R, Lao L and Osborne T 1999 *Physical Review Letters* **82** 3811

[2] Politzer P A, Petty C C, Jayakumar R J, Luce T C, Wade M R, Deboo J C, Ferron J R, Gohil P, Holcomb C T, Hyatt A W, Kinsey J, L a Haye R J, Makowski M A and Petrie T W 2008 *Nucl. Fusion* **48** 075001

[3] Gerhardt S P, Brennan D P, Buttery R, L a Haye R J, Sabbagh S, Strait E, Bell M, Bell R, Fredrickson E, Gates D, Leblanc B, Menard J, Stutman D, Tritz K and Yuh H 2009 *Nucl. Fusion* **49** 032003

[4] Berkery J W, Sabbagh S A, Betti R, Hu B, Bell R E, Gerhardt S P, Manickam J and Tritz K 2010 *Physical Review Letters* **104** 035003

[5] Sabbagh S A, Berkery J W, Bell R E, Bialek J M, Gerhardt S P, Menard J E, Betti R, Gates D A, Hu B, Katsuro-Hopkins O N, Leblanc B P, Levinton F M, Manickam J, Tritz K and Yuh H 2010 *Nucl. Fusion* **50** 025020

[6] L a Haye R J, Petty C C, Politzer P A and Team t D D 2011 *Nucl. Fusion* **51** 053013

[7] Park Y S, Sabbagh S A, Bialek J M, Berkery J W, Lee S G, Ko W H, Bak J G, Jeon Y M, Park J K, Kim J, Hahn S H, Ahn J W, Yoon S W, Lee K D, Choi M J, Yun G S, Park H K, You K I, Bae Y S, Oh Y K, Kim W C and Kwak J G 2013 *Nucl. Fusion* **53** 083029

[8] Burrell K H 1997 *Phys. Plasmas* **4** 1499

[9] Hinton F and Wong S 1985 *Physics of Fluids* **28** 3082

[10] Angioni C, Casson F, Veth C and Peeters A 2012 *Phys. Plasmas* **19** 122311

[11] Angioni C and Helander P 2014 *Plasma Phys. Controlled Fusion* **56** 124001

[12] Moyer R A, Paz-Soldan C, Nazikian R, Orlov D M, Ferraro N M, Grierson B A, Knölker M, Lyons B C, Mckee G R, Osborne T H, Rhodes T L, Meneghini O, Smith S, Evans T E, Fenstermacher M E, Groebner R J, Hanson J M, La Haye R J, Luce T C, Mordijck S, Solomon W M, Turco F, Yan Z, Zeng L and DIII-D Team 2017 *Phys. Plasmas* **24** 102501

[13] Garofalo A M, Solomon W M, Park J K, Burrell K H, Deboo J C, Lanctot M J, Mckee G R, Reimerdes H, Schmitz L, Schaffer M J and Snyder P B 2011 *Nucl. Fusion* **51** 083018

[14] Rice J E, Ince-Cushman A, Degrassie J S, Eriksson L G, Sakamoto Y, Scarabosio A, Bortolon A, Burrell K H, Duval B P, Fenzi-Bonizec C, Greenwald M J, Groebner R J, Hoang G T, Koide Y, Marmar E S, Pochelon A and Podpaly Y 2007 *Nucl. Fusion* **47** 1618

[15] Muller S H, Boedo J A, Burrell K H, Degrassie J S, Moyer R A, Rudakov D L, Solomon W M and Tynan G R 2011 *Phys. Plasmas* **18** 072504

[16] Muller S H, Boedo J A, Burrell K H, Degrassie J S, Moyer R A, Rudakov D L and Solomon W M 2011 *Physical Review Letters* **106** 115001

[17] Boedo J A, Degrassie J S, Grierson B, Stoltzfus-Dueck T, Battaglia D J, Rudakov D L, Belli E A, Groebner R J, Hollmann E, Lasnier C, Solomon W M, Unterberg E A, Watkins J and Team D D 2016 *Phys. Plasmas* **23** 092506

[18] Grierson B A, Chrystal C, Haskey S R, Wang W X, Rhodes T L, Mckee G R, Barada K, Yuan X, Nave M F F, Ashourvan A and Holland C 2019 *Phys. Plasmas* **26** 042304

[19] Degrassie J S 2009 *Plasma Phys. Controlled Fusion* **51** 124047

[20] Peeters A, Angioni C, Bortolon A, Camenen Y, Casson F, Duval B, Fiederspiel L, Hornsby W, Idomura Y and Hein T 2011 *Nucl. Fusion* **51** 094027

[21] Ida K and Rice J E 2014 *Nucl. Fusion* **54** 045001

[22] Rice J E 2016 *Plasma Phys. Controlled Fusion* **58** 083001

[23] Degrassie J S, Solomon W M, Rice J E and Noterdaeme J M 2016 *Phys. Plasmas* **23** 082501

[24] Rice J E, Hughes J W, Diamond P H, Cao N, Chilenski M A, Hubbard A E, Irby J H, Kosuga Y, Lin Y, Metcalf I W, Reinke M L, Tolman E A, Victora M M, Wolfe S M and Wukitch S J 2017 *Nucl. Fusion* **57** 116004

[25] Stoltzfus-Dueck T 2012 *Physical Review Letters* **108** 065002

[26] Ashourvan A, Grierson B A, Battaglia D J, Haskey S R and Stoltzfus-Dueck T 2018 *Phys. Plasmas* **25** 056114

[27] Chrystal C, Grierson B A, Solomon W M, Tala T, Degrassie J S, Petty C C, Salmi A and Burrell K H 2017 *Phys. Plasmas* **24** 042501

[28] Chrystal C, Grierson B A, Staebler G M, Petty C C, Solomon W M, Degrassie J S, Burrell K H, Tala T and Salmi A 2017 *Phys. Plasmas* **24** 056113

[29] Staebler G M and John H E S 2006 *Nucl. Fusion* **46** L6–L8

[30] Budny R V, Andre R, Bateman G, Halpern F, Kessel C E, Kritz A and Mccune D 2008 *Nucl. Fusion* **48** 075005

[31] Halpern F D, Kritz A H, Bateman G, Pankin A Y, Budny R V and McCune D C 2008 *Phys. Plasmas* **15** 062505

[32] Paul E J, Landreman M, Poli F M, Spong D A, Smith H M and Dorland W 2017 *Nucl. Fusion* **57** 116044

[33] Petty C 2008 *Phys. Plasmas* **15** 080501

[34] Luce T C, Petty C C and Cordey J G 2008 *Plasma Phys. Controlled Fusion* **50** 043001

[35] deGrassie J S, Groebner R and Burrell K H 2006 *Phys. Plasmas* **13** 112507
[36] Grierson B, Burrell K H, Chrystal C, Groebner R, Kaplan D, Heidbrink W, Muñoz Burgos J, Pablant N, Solomon W and Zeeland M V 2012 *Rev. Sci. Instrum.* **83** 10D529
[37] Haskey S R, Grierson B A, Stagner L, Chrystal C, Ashourvan A, Bortolon A, Boyer M D, Burrell K H, Collins C, Groebner R J, Kaplan D H and Pablant N A 2018 *Rev. Sci. Instrum.* **89** 10D110
[38] Omotani J, Pusztai I, Newton S and Fülöp T 2016 *Nucl. Fusion* **56** 124002
[39] Omotani J T, Newton S L, Pusztai I, Viezzer E, Fülöp T and the ASDEX Upgrade Team 2017 *Nucl. Fusion* **57** 066048
[40] Rozhansky V, Kaveeva E, Voskoboynikov S, Counsell G, Kirk A, Coster D and Schneider R 2005 *Journal of Nuclear Materials* **337-339** 291–295
[41] Rozhansky V 2013 *Phys. Plasmas* **20** 101614
[42] Severo J H F, Ronchi G, Galvao R M O, Nascimento I C, Guimaraes-Filho Z O, Kuznetsov Y K, Nave M F F, Oliveira A M, Nascimento F d and Tendler M 2015 *Nucl. Fusion* **55** 093001
[43] Loarte A 2001 *Plasma Phys. Controlled Fusion* **43** R183–R224
[44] Sontag A C, Chen X, Canik J, Leonard A, Lore J D, Moser A L, Murakami M, Park J M and Petty C 2017 *Nucl. Fusion* **57** 076025
[45] Sang C F, Stangeby P C, Guo H Y, Leonard A W, Covele B, Lao L L, Moser A L and Thomas D M 2017 *Plasma Phys. Controlled Fusion* **59** 025009
[46] Wang H Q, Guo H Y, Leonard A W, Moser A L, Osborne T H, Snyder P B, Belli E, Groebner R J, Thomas D M, Watkins J G, Yan Z and group t D D 2018 *Nucl. Fusion* **58** 096014
[47] Degrassie J S, Groebner R J, Burrell K H and Solomon W M 2009 *Nucl. Fusion* **49** 085020
[48] Schneider R, Reiter D, Zehrfeld H P, Braams B, Baelmans M, Geiger J, Kastelewicz H, Neuhauser J and Wunderlich R 1992 *Journal of Nuclear Materials* **196-198** 810–815
[49] Wiesen S, Reiter D, Kotov V, Baelmans M, Dekeyser W, Kukushkin A S, Lisgo S W, Pitts R A, Rozhansky V, Saibene G, Veselova I and Voskoboynikov S 2015 *Journal of Nuclear Materials* **463** 480–484
[50] BONNIN X, DEKEYSER W, PITTS R, COSTER D, VOSKOBOYNIKOV S and WIESEN S 2016 *Plasma and Fusion Research* **11** 1403102–1403102
[51] Krasheninnikov S I, Kukushkin A S and Pshenov A A 2016 *Phys. Plasmas* **23** 055602
[52] Hawryluk R J 1980 *Phys. Plasmas Close to Thermonuclear Conditions* **1** 19
[53] Snyder P B, Groebner R J, Hughes J W, Osborne T H, Beurskens M, Leonard A W, Wilson H R and Xu X Q 2011 *Nucl. Fusion* **51** 103016
[54] Waltz R E, Staebler G M and Dorland W 1997 *Phys. Plasmas* **4** 2482
[55] Candy J, Holland C, Waltz R E, Fahey M R and Belli E 2009 *Phys. Plasmas* **16** 060704
[56] Staebler G M, Kinsey J E and Waltz R E 2007 *Phys. Plasmas* **14** 055909
[57] Kinsey J and Staebler G 2008 *Phys. Plasmas*
[58] Staebler G M, Candy J, Howard N T and Holland C 2016 *Phys. Plasmas* **23** 062518
[59] Belli E A and Candy J 2008 *Plasma Phys. Controlled Fusion* **50** 095010
[60] Meneghini O, Smith S P, Lao L L, Izacard O, Ren Q, Park J M, Candy J, Wang Z, Luna C J, Izzo V A, Grierson B A, Snyder P B, Holland C, Penna J, Lu G, Raum P, Mccubbin A, Orlov D M, Belli E A, Ferraro N M, Prater R, Osborne T H, Turnbull A D and Staebler G M 2015 *Nucl. Fusion* **55** 083008
[61] Ashourvan A private communication
[62] Grierson B A, Staebler G M, Solomon W M, Mckee G R, Holland C, Austin M, Marinoni A, Schmitz L, Pinsker R I and Team D D 2018 *Phys. Plasmas* **25** 022509
[63] Paz-Soldan C, Nazikian R, Cui L, Lyons B C, Orlov D M, Kirk A, Logan N C, Osborne T H, Suttrop W and Weisberg D B 2019 *Nucl. Fusion* **59** 056012
[64] Lanctot M J, Snipes J A, Reimerdes H, Paz-Soldan C, Logan N, Hanson J M, Buttery R J, Degrassie J S, Garofalo A M, Gray T K, Grierson B A, King J D, Kramer G J, L a Haye R J, Pace D C, Park J K, Salmi A, Shiraki D, Strait E J, Solomon W M, Tala T and Van Zeeland M A 2017 *Nucl. Fusion* **57** 036004